Case Study 7

Red Tide Detection in the Eastern Gulf of Mexico Using MODIS Imagery

Chuanmin Hu*[1], Jennifer Cannizzaro[1], Kendall L. Carder[1], Zhongping Lee[2], Frank E. Muller-Karger[1] and Inia Soto[1]

7.1 Background

Many of the red tides (i.e., harmful algal blooms or HABs) in the eastern Gulf of Mexico (GOM) (24°–31°N, 90°–80°W) are caused by the toxic dinoflagellate, *Karenia brevis* (previously known as *Gymnodinium breve* or *G. breve*). Brevetoxins produced during *K. brevis* blooms can kill fish, mammals, and other marine organisms and cause respiratory irritation in humans (Hemmert, 1975; Asai et al., 1982; Landsberg and Steidinger, 1998; Kirkpatrick et al., 2004; Flewelling et al., 2005). *K. brevis* blooms can also adversely impact local tourism and commercial shellfish industries, leading to economic losses that have exceeded millions of US dollars during a single bloom event (Habas and Gilbert, 1974; Larkin and Adams, 2007).

Although *K. brevis* blooms can change the water to many different colours (e.g., brown, red, or even black) depending on the bloom's cell concentration and the concentration of other important optical constituents (Dierssen et al., 2006), they are commonly referred to as red tides. In the eastern GOM, red tides occur every year, mainly from late summer to early spring, yet their occurrence frequency, intensity, spatial extent, and duration all vary from year to year. Despite many years of community efforts, the mechanisms of initiation, maintenance and demise of red tides are still poorly understood and require further investigation. Data collected between the 1950's and the 1980's suggest that red tides are initiated offshore in nutrient-poor waters (Tester and Steidinger, 1997), and that they move toward shore by winds and currents, where they concentrate near fronts and utilize new nutrients from coastal runoff (Walsh et al., 2006). Several hypotheses that attempt to explain new nutrient supplies for these HABs have been proposed, including nitrogen fixation stimulated by atmospheric deposition of iron-rich Saharan dust particles

[1]College of Marine Science, University of South Florida, 140 7th Ave., S., St. Petersburg, FL 33701, USA. **Email address:* hu@marine.usf.edu

[2]Geosystems Research Institute, Mississippi State University, Stennis Space Center, MS 39529, USA

(Lenes et al., 2001; Walsh and Steidinger, 2001; Walsh et al., 2006), submarine groundwater discharge (Hu et al., 2006), and dead fish (Walsh et al., 2009). These hypotheses remain to be tested, and these possible sources need to be evaluated relative to sources such as upwelling of deeper GOM waters, riverine inputs, and benthic nutrient regeneration.

Timely information of *K. brevis* blooms is essential for all aspects of red tide studies, including testing hypotheses, assessing and managing the coastal environment, and forecasting and mitigation of red tides. In the past few decades, several long-term monitoring programs have invested significant resources in collecting red tide information. These include the Monitoring and Event Response for Harmful Algal Blooms (MERHAB) program supported by the U.S. NOAA (National Oceanic and Atmospheric Administration) and the Florida Fish and Wildlife Research Institute, several other programs supported by the state of Florida, local environmental groups, and volunteers. Most of these efforts rely on water sample analysis from field surveys because this is currently the only accurate means to differentiate *K. brevis* from other phytoplankton species. However, field surveys are often limited in spatial coverage and temporal frequency, especially during severe weather events. This lack of synoptic and frequent field observations makes it difficult to 1) provide near real-time information for rapid response, and 2) understand the long-term red tide occurrence statistics. For example, there has been substantial discussion and debate within the scientific community as to whether there is any historical trend in red tide occurrence along the west-central Florida coast. While Brand and Compton (2007) found that the frequency and duration of red tides appear to have increased in recent years, there was also argument (Christman and Young, 2006; Alcock, 2007) that this observation may simply be due to the unevenly distributed sampling scheme, the so-called observer effect (i.e. increased sampling during recent years because of increased public and scientific awareness - http://research.myfwc.com/features/view_article.asp?id=27095).

In addition to the intensive field sampling efforts, satellite remote sensing can offer synoptic and more frequent measurements, with imagery available in near real-time (Babin et al., 2008). Therefore, detection of red tides via remote sensing is highly desirable, and thus has been an active research topic. Satellite imagery already has been used for operational monitoring of HABs in the GOM region. Some of the disadvantages are that satellite remote sensing using visible radiance is limited by cloud cover, spatial resolution, lack of information with depth below the surface, and algorithm uncertainty. While the first three are inherent with a given satellite-based instrument and cannot be fully "corrected", there has been continuous progress in algorithm development to improve the accuracy in red tide detection. Here, using several examples, we demonstrate how to use Moderate Resolution Imaging Spectroradiometer (MODIS) satellite imagery to differentiate the various waters, including *K. brevis* red tides in the eastern GOM. We will begin by reviewing briefly the underlying principles of red tide detection from space, and

follow with descriptions of the data and methods. We show several examples to illustrate the potential of this technology.

7.1.1 Principles

The use of ocean-colour satellites for rapid detection of red tides in the eastern GOM has been described previously (e.g., Stumpf et al., 2003a; Tomlinson et al., 2004; 2008; Hu et al., 2005; Cannizzaro et al., 2008; Amin et al., 2009). *K. brevis* cells contain chlorophyll-*a* and accessory pigments. These pigments have reflectance spectra that allow them to be differentiated from other water constituents, such as suspended non-living particles. The chlorophyll-*a* content of *K. brevis* cells ranges from ~8.5 pg/cell for natural populations to ~25 pg/cell for cultured populations (Evens et al., 2001). Assuming 10 pg/cell, a concentration of $2x10^4$ cells l^{-1} implies 0.2 mg m^{-3} of chlorophyll-*a*, close to the clear-water background chlorophyll-*a* concentration (Chl-*a*) in the eastern GOM. Satellite ocean-colour instruments typically have a measurement precision (not accuracy) of 0.01 – 0.02 mg m^{-3} for blue waters. In order for a *K. brevis* bloom to be detected and identified as such, however, Chl-*a* needs to exceed 0.5 – 1 mg m^{-3}, corresponding to *K. brevis* cell concentrations of $5x10^4$ to 10^5 cells l^{-1}. These concentrations are high enough to cause fish kills (Steidinger et al., 1998).

Satellite-derived Chl-*a* data products can be used to identify areas of possible red tides. For example, a Chl-anomaly technique was proposed by Stumpf et al. (2003a) to flag "new" blooms in an area relative to conditions two weeks earlier — under certain conditions these new blooms can be flagged as potential *K. brevis* blooms.

There are practical difficulties when applying the Chl-based approach to identify red tides in the eastern GOM using remote sensing data. The first is the difficulty with obtaining an accurate chlorophyll estimate in many coastal waters because of errors in the atmospheric correction algorithms (to remove atmospheric effects from the spectral satellite signal) and bio-optical inversion algorithms (to convert the surface spectral signal to Chl-*a* and other bio-optical parameters). In these waters, the optical signal may not be dominated by phytoplankton, but instead by coloured dissolved organic matter (CDOM) from *in situ* phytoplankton degradation or terrestrial runoff, resuspended sediments, and/or the bottom effects in clear, shallow water. The empirical band-ratio OC4 algorithm (O'Reilly et al., 2000; version 4) that is used to convert the surface spectral signal to Chl-*a* does not differentiate between optically important constituents, but rather regards all influences as originating from Chl-*a*. This causes large errors in the Chl-*a* estimates for the eastern GOM coastal waters (Hu et al., 2003; 2005). Although a semi-analytical algorithm designed for MODIS (Carder et al., 1999) can separate CDOM from Chl-*a* and thus improve Chl-*a* estimates in clear and moderately turbid waters (Hu et al., 2003), in highly turbid coastal waters the algorithm switches to an empirical blue/green band-ratio form.

The second difficulty is differentiating *K. brevis* blooms from other phytoplankton blooms. Chl-*a* cannot be used for this task because both types of blooms contain high Chl-*a*. Discrimination between *K. brevis* and other phytoplankton groups using *in situ* optical observations has been done with some success (Cullen et al., 1997; Millie et al., 1997; Lohrenz et al., 1999; Schofield et al., 1999; Kirkpatrick et al., 2000). However, these techniques require hyperspectral data (e.g., Craig et al., 2006), which are not available from satellites. Several HAB detection techniques have been proposed that can use multi-spectral satellite data. These include methods involving particulate backscattering (Cannizzaro et al., 2008), spectral curvature (Tomlinson et al., 2008), a combination of red-wavelength bands (Amin et al., 2009), and image segmentation (Zhang et al., 2002).

In this demonstration, we will combine the techniques proposed by Hu et al. (2005) and Cannizzaro et al. (2008). We used MODIS satellite data to show how to differentiate bloom waters from coastal waters in which other constituents dominate the optical signal, and to differentiate *K. brevis* blooms from other blooms. Specifically, we distinguished phytoplankton blooms from CDOM-rich waters by examining spectral water-leaving radiance and solar stimulated fluorescence (Hu et al., 2005), and *K. brevis* blooms were distinguished from non-*K. brevis* blooms by examining bloom backscattering efficiency (Cannizzaro et al., 2008).

7.2 Data and Methods

MODIS Level-1a data were obtained from the U.S. NASA Goddard Space Flight Center (GSFC) (`http://oceancolor.gsfc.nasa.gov`). These data are open to the public within a few hours (typically 3 – 6) of collection by the spacecraft. The following steps were used to generate georeferenced MODIS images at 1-km resolution:

1. MODIS/Aqua Level-1a data were processed to generate Level-1b (calibrated total radiance) data for the "ocean colour" spectral wavebands in the visible and near-infrared, and geolocation data using SeaWiFS Data Analysis System (SeaDAS) software. The 1-km bands were designed for the ocean with sufficient sensitivity to detect subtle changes in ocean colour. The Level-1b and geolocation data were stored in computer files in HDF (Hierarchical Data Format);
2. MODIS Level-1b data were atmospherically corrected to generate the spectral remote sensing reflectance ($R_{rs}(\lambda)$, sr^{-1}) and normalized water-leaving radiance (nLw(λ), mW cm^{-2} μm^{-1} sr^{-1}) using SeaDAS. These two parameters can be derived from each other using the extraterrestrial solar irradiance (time-independent constants). During this step, ancillary data (surface wind, pressure, total ozone thickness, and atmospheric water vapor content) were downloaded from NASA/GSFC and used to estimate the atmospheric contribution to the satellite-received radiance. The atmospheric correction was based on the two near-infrared (NIR) bands at 748 nm and 869 nm, from which atmo-

spheric properties were derived and used to estimate the properties at other wavelengths on a per-pixel basis (Gordon and Wang, 1994). Over turbid coastal waters, a modification to the atmospheric correction scheme was used that involves using an iterative approach to account for the non-zero water-leaving radiance in the NIR (Stumpf et al., 2003b);

3. The spectral $R_{rs}(\lambda)$ was used to derive two data products: Chl-*a* from an empirical band-ratio algorithm (OC4v4; O'Reilly et al., 2000); particulate backscattering coefficient at 551 nm (b_{bp},551) using a Quasi-Analytical Algorithm (QAA, Lee et al., 2002). Using nLw(λ) data from three MODIS wavebands at 667, 678, and 748 nm we derived the Fluorescence Line Height (FLH, mW cm^{-2} μm^{-1} sr^{-1}) product using a linear baseline algorithm (Letelier et al., 1996). Further, the empirically-derived Chl-*a* was used to estimate the particulate backscattering coefficient at 551 nm using the Morel (1988) algorithm, designed for phytoplankton dominated (i.e., Case 1) waters:

$$b_{bp,Morel} = 0.3 \times \text{Chl}^{0.62} \times (0.002 + 0.02 \times (0.5 - 0.25 \times \log_{10}\text{Chl})) \qquad (7.1)$$

4. These products $R_{rs}(\lambda)$, nLw(λ), Chl-*a*, $b_{bp,QAA}$, $b_{bp,Morel}$ and FLH) were georeferenced to a cylindrical equidistant (rectangular, also called geographic lat/lon) projection for the area of interest. The final images had a spatial resolution equivalent to 1-km per image pixel. The map-projected products were stored in HDF files. Individual products were also converted to raster image formats with an embedded palette using pre-defined colour look-up tables;
5. nLw(λ) data at 551, 488, and 443 nm were used as the red, green and blue channels to compose an Enhanced RGB (ERGB) image. The red waveband (667 nm) was not used because water-leaving radiance at this wavelength (nLw(667)) is very low except in sediment-rich waters, thus providing little information on red tides.

The Florida Fish and Wildlife Research Institute (FWRI) has compiled an *in situ* database for *K. brevis* cell concentration data. Water samples have been collected by various research and volunteer groups in the eastern GOM and analyzed using microscopic enumeration techniques. These data, although not continuous in either space or time, were used as ground-truth to help interpret the MODIS imagery. Below we demonstrate, step by step, how the various colour features are identified and interpreted from the MODIS imagery.

7.3 Demonstration

In 2005, a long-lasting, extensive red tide event occurred on the west Florida shelf (WFS, 24.5°–30.1°N and 85.1°–81.5°W), which may have been related to excessive rainfall in both 2004 and 2005 (Hu et al., 2006). The event started in January 2005

near Tampa Bay, Florida (Tampa Bay is marked as "A" in Figure 7.1a). Figure 7.1 shows several MODIS products from a scene collected on 21 January 2005, where the red tide patch can be seen.

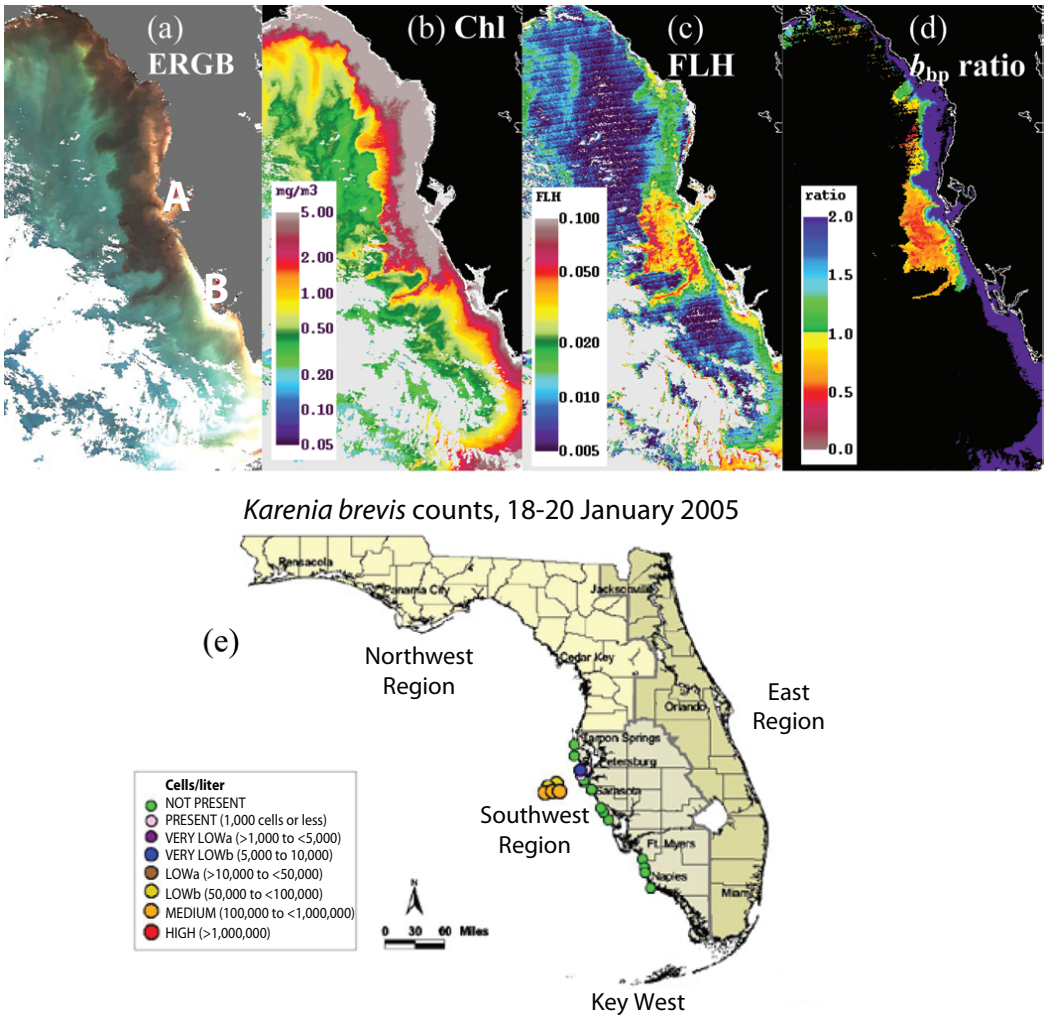

Figure 7.1 (a – d) MODIS images on 21 January 2005 showing a *K. brevis* bloom in coastal waters between Tampa Bay (A, 27.75°N, 82.56°W) and Charlotte Harbor (B, 26.75°N, 82.1°W). The images cover the area between approximately 24.5°–30.1°N and 85.1°–81.5°W. The various image types were generated using Steps 1 – 5 described in the Data and Methods section. In (d), the b_{bp} ratio is defined as $b_{bp,QAA}/b_{bp,Morel}$ (e) *K. brevis* concentration (in cells l^{-1}) obtained from FWRI (http://research.myfwc.com/gallery/image_details.asp?id=24764).

Figure 7.1a shows an ERGB image, where the dark colours result from increased light absorption in the blue wavelength (443 nm) due to high concentrations of CDOM and/or chlorophyll-*a*, and bright colours (light blue, yellow and white) result from suspended sediments and/or shallow bottom. The corresponding Chl-*a* image

in Figure 7.1b, derived from the blue-green band ratio algorithm, shows erroneously elevated Chl-*a* along the entire coast. In contrast, the FLH image in Figure 7.1c helps distinguish dark CDOM-rich waters (erroneously interpreted as high Chl-*a* in band ratio algorithms) from phytoplankton-rich waters. FLH is insensitive to CDOM (McKee et al., 2007). However, FLH is not a reliable parameter in sediment-rich waters (Gilerson et al., 2007). The high FLH values near Charlotte Harbor (Charlotte Harbor is marked as "B" in Figure 7.1a) for example, may in part be false interpretation of suspended sediments.

Figure 7.1 reveals: 1) Chl-rich waters (dark colour in ERGB with high FLH values); 2) CDOM-rich waters (dark colour in ERGB with low FLH values); 3) sediment-rich waters (bright colour in ERGB with high FLH values); and 4) shallow, clear waters (bright colour in ERGB with low FLH values). Of these, observations 3 and 4 are sometimes difficult to distinguish from each other, especially for very shallow waters (< 5 m water depth) because nLw in the fluorescence bands may also be influenced by benthic algae or sediments. This should not affect our interpretation because both cases are excluded as potential *K. brevis* blooms. Of the four, observation 1 represents waters with high biomass (Chl-*a*) and therefore can be *K. brevis* or other blooms. However, there are two drawbacks from this interpretation. The first is its qualitative nature. Indeed, the terms "high" and "low" only provide a relative sense. The second drawback is that it is impossible to tell if the high-FLH dark waters contain high concentrations of the toxic *K. brevis* or other phytoplankton species (such as diatoms).

To overcome these two difficulties, we first assume that FLH > 0.015 – 0.02 mW cm^{-2} μm^{-1} sr^{-1} can indicate bloom conditions and FLH < 0.01 – 0.015 represent non-bloom conditions (note that the values between 0.01 and 0.02 represent transition conditions). Observations from South Florida coastal waters suggest that a FLH value of 0.01 mW cm^{-2} μm^{-1} sr^{-1} is equivalent to about 1 mg m^{-3} Chl-*a* for the range of 0.4 – 4 mg m^{-3} ($Chl = 1.255 \times (FLH \times 100)^{0.86}$, r=0.92, n=77, Hu et al., 2005), although the relationship between FLH and Chl-*a* (a function of fluorescence efficiency) varies.

The technique proposed by Cannizzaro et al. (2008) was then used to examine the backscattering coefficient at 551 nm ($b_{bp,551}$) estimated with the QAA algorithm (Lee et al., 2002) in reference against $b_{bp,Morel}$ from a Case-1 empirical algorithm (Morel, 1988; Equation 7.1). Results are shown in Figure 7.1d. To exclude non-productive waters, pixels with Chl-*a* < 1.5 mg m^{-3} are masked as black. Because *K. brevis* blooms exhibit a lower backscattering efficiency compared to diatom blooms, the warm colours (yellow-red, with $b_{bp,551}/b_{bp,Morel} < 1.0$) in Figure 7.1d represent potential *K. brevis* blooms. Indeed, near concurrent *in situ* water sample analysis from FWRI confirms this finding (Figure 7.1e), where waters offshore of Tampa Bay showed medium concentrations of *K. brevis* cells (100,000 to <1,000,000 cells l^{-1}). Further, in nearshore waters there were no *K. brevis* found in these samples, consistent with the high b_{bp} ratios shown in Figure 7.1d. In other words, the high-

FLH values near Charlotte Harbor (sediment-rich water as identified by the bright colour in Figure 7.1a) is successfully discarded as potential *K. brevis* blooms in Figure 7.1d.

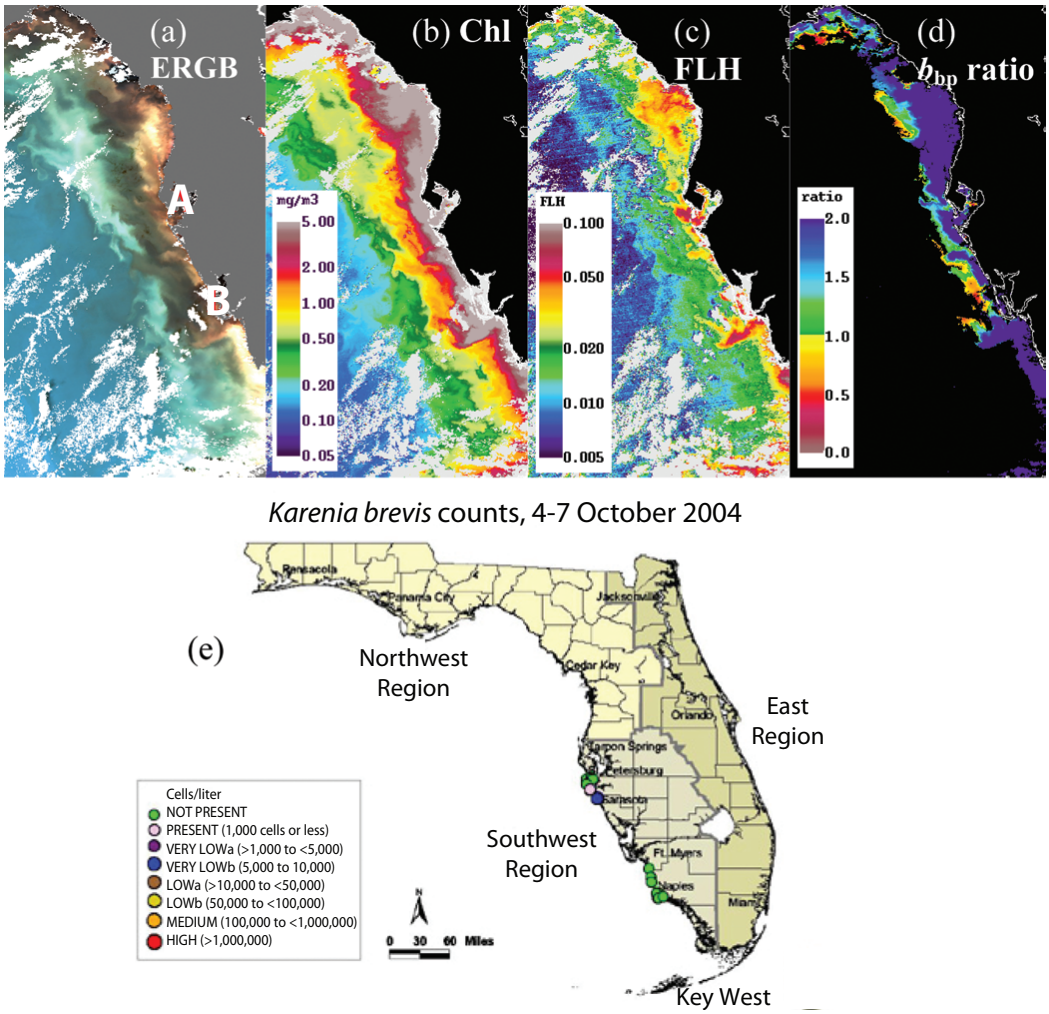

Figure 7.2 (a – d) MODIS images on 1 October 2004 showing diatom blooms off Tampa Bay (A, 27.75°N, 82.56°W) and Charlotte Harbor (B, 26.75°N, 82.1°W). The images cover the area between approximately 24.5°–30.1°N and 85.1°–81.5°W. The various image types were generated using Steps 1 – 5 described above in the Data and Methods section. In (d), the b_{bp} ratio is defined as $b_{bp,QAA}/b_{bp,Morel}$ (e) *K. brevis* concentration (in cells l^{-1}) obtained from FWRI (http://research.myfwc.com/gallery/image_details.asp?id=20058).

While Figure 7.1 demonstrates the multiple steps used to delineate *K. brevis* blooms in optically complex waters on the west Florida Shelf, Figure 7.2 shows another case where the same technique is used to identify non-*K. brevis* (in this case, diatom) blooms. Figure 7.2a shows that, in less than one week after Hurricane Jeanne's passage on 26 September 2004, most of the west Florida Shelf waters

became enriched in CDOM/Chl-*a* and suspended sediments, all interpreted as high Chl-*a* (Figure 7.2b). While the FLH image in Figure 7.2c shows potential blooms in nearshore waters, especially near the Tampa Bay and Charlotte Harbor mouths, the b_{bp} ratio image in Figure 7.2d indicates the possibility that these nearshore blooms are *K. brevis* blooms, is low. Although concurrent water sample data lack coverage of most shelf waters, the limited data in Figure 7.2e confirms that the high FLH patches near Tampa Bay and Charlotte Harbor mouths are non-*K. brevis* blooms. Indeed, the FWRI database showed 0 cells l^{-1} of *K. brevis* but very high levels (up to 230,000 cells l^{-1}) of *Pseudonitzschia* (a toxic diatom) in water samples collected from piers/beaches off Tampa Bay (e.g. Mullet Key, Anna Maria Island, Skyway fishing pier, offshore Egmont Key) between 2–7 October 2004. In this case, the image set used here not only identifies blooms, but also recognizes non-*K. brevis* blooms. Combined with the results shown in Figure 7.1, we can conclude that this technique is efficient, at least for the two cases presented here, in delineating the following waters: Chl-rich, sediment-poor waters; CDOM-rich, Chl-poor waters; sediment-rich and/or shallow, clear waters; *K. brevis* and other bloom waters.

7.4 Training

To help prepare and interpret MODIS imagery, we now go through each step to generate the various types of MODIS images from a map-projected MODIS Level-3 HDF data file. The MODIS data (Figure 7.3) were collected on 7 October 2006, where ERGB, Chl-*a*, FLH, and b_{bp} ratio images are presented in Figures 7.3a-d, respectively. The following steps were used in SeaDAS for image generation, visualization, and interpretation, but any other software package that has basic image processing capabilities and HDF compatibility can also be used.

Step 1: Download the MODIS Level-3 HDF data file from the IOCCG website (`http://www.ioccg.org/handbook/Hu_red/`) and open in a SeaDAS Display window. Load the three bands nLw_443, nLw_488, and nLw_551 in the "Band List Selection Window." Then, under Utilities => Data Visualization => Load True Color Image, choose "Band List" instead of "Input File." Choose band numbers 3, 2, 1, for the R, G, B channels, respectively. Enter 10 for slopes and 0 for intercepts. Load the RGB channels in the "Band List Selection" window, and display the true colour image. An image similar to Figure 7.3a should appear in a separate window. A high-resolution coastline can be overlaid on the image by selecting Setups => Coastline. The final image can be saved as an 8-bit png image (colour coded 2-dimensional image) or a 24-bit png image (3-dimensional image) under Functions => Output => Display.

Step 2: Use the same method in Step 1 above to load the "chlor_a" data product from the HDF file into the "Band List Selection Window," and display the image in a separate window. The colour shades in this window appear strange because of the

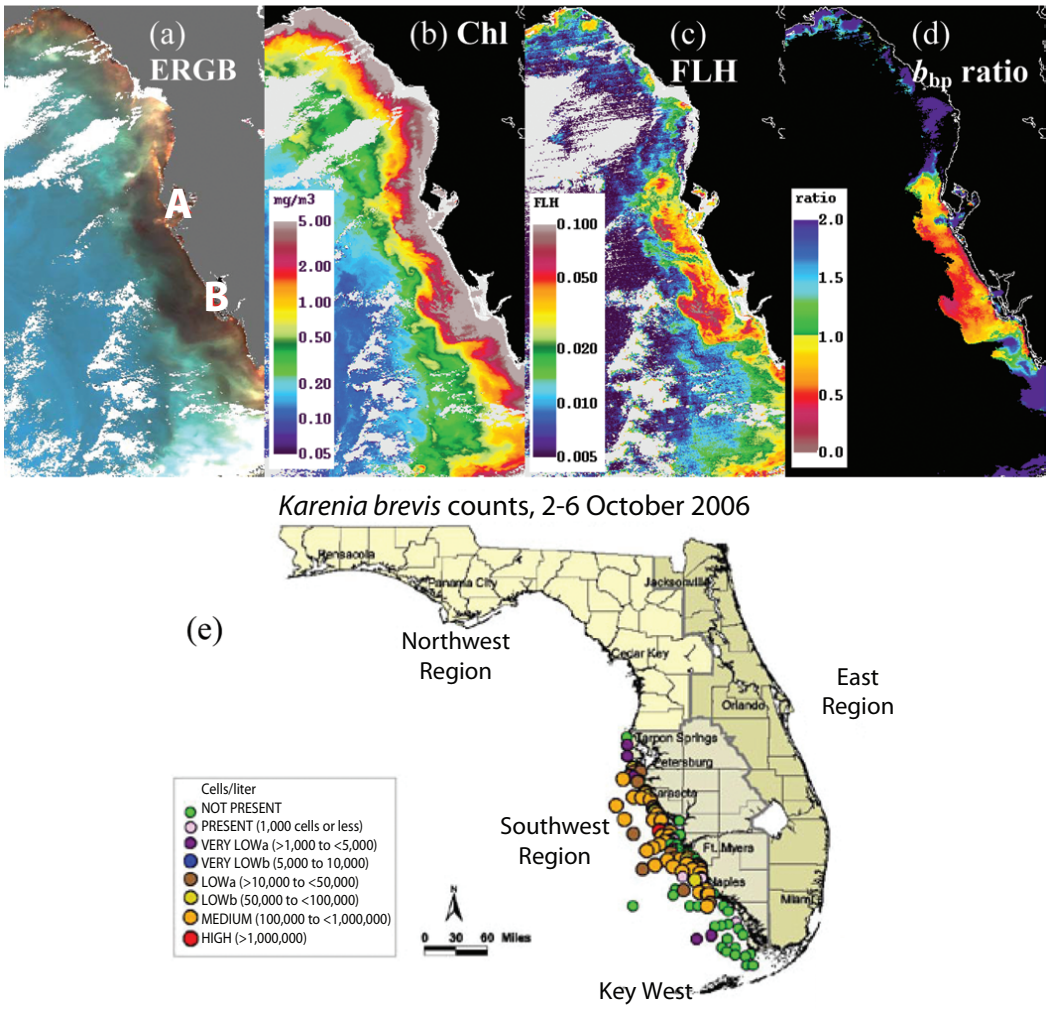

Figure 7.3 (a – d) MODIS images on 7 October 2006 showing *K. brevis* blooms off the central west Florida between Tampa Bay (A, 27.75°N, 82.56°W) and Charlotte Harbor (B, 26.75°N, 82.1°W). The images cover the area between approximately 24.5°–30.1°N and 85.1°–81.5°W. The various image types were generated using Steps 1 – 5 described in the Data and Methods section. In (d), the b_{bp} ratio is defined as $b_{bp,QAA}/b_{bp,Morel}$ (e) *K. brevis* concentration (in cells l^{-1}) obtained from FWRI (http://research.myfwc.com/gallery/image_details.asp?id=24504.

colour encoding in Step 1. The colour scheme can be changed to a "rainbow" colour by selecting "Chlorophyll a" in the list of colours from Functions => Color Lut => Load Lut. The Chl-*a* image with this colour scheme may appear different to that in Figure 7.3b, but the colour stretch can be adjusted by selecting Functions => Rescale with a log stretch. A colour legend can be added by selecting Functions => Color Bar => On, and a high-resolution coastline can also be added using methods in Step 1. The final image can be saved as a colour-coded png image, similar to Step 1.

Step 3: The same steps as in Step 2 are used to load the "flh" data product from the HDF file, display it in a separate window, adjust the colour stretch, and save it as a colour-coded png image. Note that to show details at low values, a logarithmic colour stretch is required under Functions => Rescale.

Step 4: The SeaDAS software allows a user to define a new parameter using existing parameters. Based on the "chlor_a" data available in the "Band List Selection" window, Equation 7.1 is used to estimate $b_{\text{bp,Morel}}$. Assuming "chlor_a" is the 5^{th} band in the band list, type in the following commands under Utilities => Data Manipulation => User Defined Operations:

```
bad_idx=where(B5 lt 0.001)
B5[bad_idx]=0.001
result=0.3*B5^0.62*(0.002 + 0.02 * (0.5 - 0.25 * alog10(B5)))
```

Then, type in "bbp_morel" in the "New band name" field, and click "Run." This will create a new parameter "bbp_morel" in the "Band List Selection" window (assuming it is the 6^{th} band in the window). Load bbp_551_qaa from the HDF file to this window (assuming it is the 7^{th} band in the window). In the "User Defined Operations" window type in the following commands:

```
result=B7/B6
low_chl_idx = where(B5 lt 1.5)
result[low_chl_idx]=0.0
```

Then, type in "bbp_ratio" in the "New band name" field, and click "Run." This will create a new parameter "bbp_ratio" in the "Band List Selection" window. This band can be displayed, colour stretched, and saved as a colour-coded png image (together with a colour legend) using the same steps as above. The saved image should appear as the opposite of Figure 7.3d with the cold colours representing low values and the warm colours representing high values.

7.5 Questions

Q1: What do the various colour shades in Figure 7.3a mean? Do the dark shades between Tampa Bay and Charlotte Harbor indicate high Chl-*a*?

Q2: Do the high Chl-*a* values (yellowish and reddish colours indicated on the colour legend) in Figure 7.3b represent high chlorophyll-*a* concentrations or something else?

Q3: What do the high FLH values in Figure 7.3c mean?

Q4: Do the low "bbp_ratio" values in Figure 7.3d indicate *K. brevis* blooms?

7.6 Answers

A1: Similar to Figure 7.1a, the various colour shades in the RGB image can be used to qualitatively distinguish various waters. Dark colours result from high concentrations of CDOM and/or chlorophyll-*a*, but it is impossible to tell which of the two is dominant because they both strongly absorb blue light. So the dark shades between Tampa Bay and Charlotte Harbor do not necessarily indicate high Chl-*a*. The bright colours in the ERGB image result from suspended sediments and/or shallow bottom because they both strongly scatter light.

A2: The warm colours in coastal waters do not necessarily indicate high Chl-*a* because the band-ratio empirical algorithm used to derive Chl-*a* could falsely interpret other water constituents (CDOM, suspended sediments, and shallow bottom) as chlorophyll-*a*.

A3: While FLH is a reliable measure of biomass (Chl-*a*) in sediment-poor waters, in sediment-rich waters high FLH values may be simply due to high turbidity and not due to high Chl-*a*. Thus, combining Figure 7.3c with Figure 7.3a where sediment-rich waters can be easily identified, we can infer that high FLH values associated with dark waters in Figure 7.3a (between Tampa Bay and Charlotte Harbor) are likely associated with high biomass, while high FLH values associated with bright waters in Figure 7.3a (in the northern and southern parts of the coastal waters) are likely associated with high concentrations of suspended sediments.

A4: The low "bbp_ratio" values in Figure 7.3d very likely indicate *K. brevis* blooms. These blooms have a lower backscattering efficiency compared with non-*K. brevis* blooms. The waters with bbp_ratio < 1 can be classified as dominated by *K. brevis* cells. Indeed, analysis of near-concurrent FWRI water sample data (Figure 7.3e) confirms this inference for coastal waters between Tampa Bay and Charlotte Harbor. However, it is unknown if waters in the northern part of Florida (associated also with low bbp_ratio but high FLH) contain high concentrations of *K. brevis*, because CDOM interference to MODIS Chl may lead to erroneously overestimated Chl and lower-than-real bbp ratio. A related case can be found in Figure 7.1d, where offshore waters north of Tampa Bay show high CDOM (Figure 7.1a) and erroneously high MODIS Chl (Figure 7.1b and c), leading to low bbp_ratio with high Chl. Cross-examination of all four types of imagery is necessary to rule out potential false positive detection.

7.7 Discussion and Summary

We demonstrated the principles of *K. brevis* bloom detection using a combination of MODIS imagery and techniques proposed by Hu et al. (2005) and Cannizzaro et al. (2008). Several other methods have been published (Stumpf et al., 2003a; Tomlinson et al., 2004; 2008; Amin et al., 2009), but our purpose here is to show the principles as opposed to providing a comprehensive review on the various techniques.

The three cases shown here are successful examples. However, we must recognize that nature is more complex than shown here, and none of the published techniques is perfect. Indeed, our methods can result in both false-positives (i.e., identifies *K. brevis* blooms in non-bloom waters) and false negatives (i.e., identifies non-bloom in *K. brevis* bloom waters). Although the evaluation results of Tomlinson et al. (2008) show low possibilities (about 20 – 30%) for both error types if different image types are combined, such possibilities cannot be neglected.

The 70–80% success rate of the *K. brevis* bloom detection methods provides useful information in at least two aspects: 1) to document the *K. brevis* occurrence patterns in both space and time to help understand their initiation, maintenance, and control mechanisms and 2) to guide rapid response in field surveys. This capability, combined with the free availability of both MODIS data and processing software (SeaDAS), makes it particularly useful in implementing any regional satellite-based HABs monitoring system. The reader is cautioned, however, that not every HAB species contains high chlorophyll-*a* pigment or displays low backscattering efficiency. For a particular region, a regional algorithm based on the unique optical characteristics of HABs is often required.

At the time of writing, MODIS data from the Aqua satellite (afternoon pass, 2002 – present) are considered to be of science quality, but MODIS data from the Terra satellite (morning pass, 1999 – present) are provisional. The ocean colour community, especially the NASA Ocean Biology Processing Group (OBPG), is making progress by removing noise and improving calibration/retrieval algorithms for MODIS-Terra. The combined MODIS instruments will significantly increase the spatial/temporal coverage in many coastal regions, thus providing additional values in HABs monitoring. Likewise, when MERIS data (Medium Resolution Imaging Spectrometer, 2002 – present) at 300-m resolution are used, the capability to detect small-patch blooms should be enhanced. In the absence of fluorescence data (e.g., SeaWiFS is not equipped with the fluorescence bands), other techniques (e.g., Chl-anomaly or spectral curvature, see Tomlinson et al., 2008) can also be used.

In summary, ocean-colour satellite imagery is particularly useful in detecting and monitoring HAB events because of their synoptic and frequent coverage as well as the information carried in their spectral reflectance. Correct interpretation of the various image types requires sufficient knowledge in bio-optics and phytoplankton dynamics. In any case, the full potential of satellite remote sensing of HABs can only be realized through coordinated efforts between remote sensing specialists,

environmental scientists, coastal managers, and other groups.

7.7.1 Acknowledgements

This work was supported by the U.S. NASA (NNX09AE17G and NNX09AV56G), EPA (MX964754070), and NOAA (NA06NES4400004). We thank the U.S. NASA/GSFC for providing MODIS data and thank FWRI for providing *in situ K. brevis* concentration data.

7.8 References

Amin R, Zhou J, Gilerson A, Gross B, Moshary F, Ahmed S (2009) Novel optical techniques for detecting and classifying toxic dinoflagellate *Karenia brevis* blooms using satellite imagery. Opt Express 17:9126-9144

Asai S Krzanowski JJ, Anderson WH, Martin DF, Polson JB, Lockey RF, Bukantz SC, Szentivanyi A (1982) Effects of the toxin of red tide, *Ptychodiscus brevis*, on canine tracheal smooth muscle: a possible new asthma-triggering mechanism. J Allergy Clin Immunol 69: 418- 428

Babin M, Roesler CS, Cullen J J (eds) (2008) Real-time coastal observing systems for marine ecosystem dynamics and harmful algal blooms: Theory, instrumentation and modeling. UNESCO, Paris

Brand L, Compton A (2007) Long-term increase in *Karenia brevis* abundance along the Southwest Florida Coast. Harmful Algae 6:232-252

Cannizzaro JP, Carder KL, Chen FR, Heil CA, Vargo GA (2008) A novel technique for detection of the toxic dinoflagellate, *Karenia brevis*, in the Gulf of Mexico from remotely sensed ocean color data. Cont Shelf Res 28:137-158

Carder KL, Chen FR, Lee ZP, Hawes SK, Kamykowski D (1999) Semianalytic Moderate-Resolution Imaging Spectrometer algorithms for chlorophyll *a* and absorption with bio-optical domains based on nitrate- depletion temperatures. J Geophys Res 104:5403-5421

Christman, M , Young L (2006) Analysis of *Karenia brevis* Gulf Data. Final project report to Florida Wildlife Research Institute, from University of Florida, Gainsville, FL, June 2006

Craig SE, Lohrenz SE, Lee ZP, Mahoney KL, Kirkpatrick GJ, Schofield OM, Steward RG (2006) Use of hyperspectral remote sensing reflectance for detection and assessment of the harmful alga, *Karenia brevis*. Appl Optics 45:5414-5425

Cullen JJ, Ciotti AM, Davis RF, Lewis MR (1997) Optical detection and assessment of algal blooms. Limnol Oceanogr 42:1223-1239

Dierssen HM, Kudela RM, Ryan JP, Zimmerman RC (2006) Red and black tides: Quantitative analysis of water-leaving radiance and perceived color for phytoplankton, colored dissolved organic matter, and suspended sediments. Limnol Oceanogr 51:2646-2659

Evens TJ, Kirkpatrick GJ, Millie DF, Chapman DJ, Schofield OME (2001) Photophysiological responses of the toxic red-tide dinoflagellate *Gymnodinium breve* (Dinophyceae) under natural sunlight. J Plank Res 23:1177-1193

Flewelling, LJ, Naar JP, Abbott JP, Baden DG, Barros NB, Bossart GD, et al. (2005) Brevetoxicosis: red tides and marine mammal mortalities. Nature 435: 755-756

Gilerson A, Zhou J, Hlaing S, Ioannou I, Schalles J, Gross B, Moshary F, Ahmed S (2007) Fluorescence component in the reflectance spectra from coastal waters. Dependence on water composition. Optics Express 15:15702-15721

Gordon HR, Wang M (1994) Retrieval of water-leaving radiance and aerosol optical thickness over the oceans with SeaWiFS: A preliminary algorithm. Appl Optics 33:443-452

Habas EJ , Gilbert CK (1974) The economic effects of the 1971 Florida red tide and the damage it presages for future occurrences. Environ Lett 6: 139-147

Hemmert WH (1975) The public health implications of *Gymnodinium breve* red tides, a review of the literature and recent events. In: LoCicero, VR (ed), Proceedings of the First International Conference on Toxic Dinoflagellate Blooms: 489-497

Hu CM, Muller-Karger FE, Biggs DC, Carder KL, Nababan B, Nadeau D, Vanderbloemen J (2003) Comparison of ship and satellite bio-optical measurements on the continental margin of the NE Gulf of Mexico. Int J Rem Sens 24:2597-2612

Hu CM, Muller-Karger FE, Taylor CJ, Carder KL, Kelble C, Johns E, Heil CA (2005) Red tide detection and tracing using MODIS fluorescence data: A regional example in SW Florida coastal waters. Rem Sens Environ 97:311-321

Hu C, Swarzenski PW, Muller-Karger FE (2006) Hurricanes, submarine groundwater discharge, and Florida's red tides. Geophys Res Lett 33: L11601, doi:10.1029/2005GL025449

Kirkpatrick B, Fleming LE, Squicciarini D, Backer LC, Clark R, Abraham W, Benson J, Cheng YS, Johnson D, Pierce R, Zaias J, Bossart GD, Baden DG (2004) Literature review of Florida red tide: implications for human health effects. Harmful Algae 3:99-115

Kirkpatrick GJ, Millie DF, Moline MA, Schofield O (2000) Optical discrimination of a phytoplankton species in natural mixed populations. Limnol Oceanogr 45:467-471

Landsberg JH, Steidinger KA (1998) A historical review of *Gymnodium breve* red tides implicated in mass mortalities of the manatee (*Trichechus manatus* latiriostris) in Florida, USA. In: Reguera, B, Blanco J, Fernandez ML , Wyatt T (eds), Proceedings of the 8th International Conference on Harmful Algal Blooms, Vigo, Spain: 97-100

Larkin, SL , Adams CM (2007) Harmful algal blooms and coastal business: economic consequences in Florida. Soc Nat Resour 20: 849-859

Lee Z, Carder KL, Arnone RA (2002) Deriving inherent optical properties from water color: a multiband quasi-analytical algorithm for optically deep waters. Appl Opt 41: 5755-5772

Lenes JM, Darrow BP, Cattrall C, Heil CA, Callahan M, Vargo GA, Byrne RH, Prospero JM, Bates DE, Fanning KA, Walsh JJ (2001) Iron fertilization and the *Trichodesmium* response on the West Florida shelf. Limnol Oceanogr 46:1261-1277

Letelier RM, Abbott MR (1996) An analysis of chlorophyll fluorescence algorithms for the Moderate Resolution Imaging Spectrometer (MODIS). Rem Sens Environ 58:215-223

Lohrenz SE, Fahnenstiel GL, Kirkpatrick GJ, Carroll CL, Kelly KA (1999) Microphotometric assessment of spectral absorption and its potential application for characterization of harmful algal species. J Phycol 35:1438-1446

McKee D, Cunningham A , Wright D, Hay L (2007) Potential impacts of nonalgal materials on water-leaving Sun induced chlorophyll fluorescence signals in coastal waters. Appl Opt 46:7720-7729

Millie DF, Schofield O, Kirkpatrick GJ, Johnsen G, Tester PA, Vinyard BT (1997) Phytoplankton pigments and absorption spectra as potential 'Biomarkers' for harmful algal blooms: a case study of the Florida red-tide dinoflagellate, *Gymnodinium breve*. Limnol Oceanogr 42:1240-1251

Morel A (1988) Optical modeling of the upper ocean in relation to its biogenous matter content (Case I waters). J Geophys Res 93:10,749-10,768

O'Reilly JE, Maritorena S, Siegel D, O'Brien MC, Toole, D, Mitchell BG, Kahru, M, Chavez FP, Strutton P, Cota G, Hooker SB, McClain CR, Carder KL, Muller-Karger F, Harding L, Magnuson A, Phinney D, Moore GF, Aiken J, Arrigo KR, Letelier R, Culver M (2000) Ocean color chlorophyll a algorithms for SeaWiFS, OC2 and OC4: Version 4. In: Hooker SB and Firestone ER (eds) SeaWiFS Postlaunch Calibration and Validation Analyses (Part 3), NASA Technical Memorandum 2000-206892, Volume 10, NASA GSFC, 9-23

Schofield O, Grzymski J, Bisset WP, Kirkpatrick GJ, Millie DF, Moline M, Roesler CS (1999) Optical monitoring and forecasting systems for harmful algal blooms: possibility or pipe dream? J Phycol 35:1477-1496

Steidinger, KA, Vargo GA , Tester PA, Tomas CR (1998) Bloom dynamics and physiology of Gymnodinium breve, with emphasis on the Gulf of Mexico. In: Physiological Ecology of Harmful Algal Blooms (Anderson EM , Cembella AD, Hallengraff GM, eds) Springer-Verlag, New York: 135-153

Stumpf RP, Culver ME, Tester PA, Tomlinson M, Kirkpatrick GJ, Pederson BA, Truby E, Ransibrahmanakul V, Soracco M (2003) Monitoring *Karenia brevis* blooms in the Gulf of Mexico using satellite ocean color imagery and other data. Harmful Algae 2:147-160

Stumpf RP, Arnone RA, Gould RW, Martinolich PM, Ransibrahmanakul V (2003b) A partially coupled ocean-atmosphere model for retrieval of water-leaving radiance from SeaWiFS in coastal waters.

In: S B Hooker and E R Firestone (eds) SeaWiFS postlaunch technical report series, Vol 22: Algorithm updates for the fourth SeaWiFS data processing, 51-59

Tester PA, Steidinger KA (1997) *Gymnodinium breve* red tide blooms: Initiation, transport, and consequences of surface circulation. Limnol Oceanogr 42:1039-1051

Tomlinson MC, Stumpf RP, Ransibrahmanakul V, Truby EW, Kirkpatrick GJ, Pederson BA, Vargo GA, Heil CA (2004) Evaluation of the use of SeaWiFS imagery for detecting *Karenia brevis* harmful algal blooms in the eastern Gulf of Mexico. Rem Sens Environ 91:293-303

Tomlinson MC, Wynne TT, Stumpf RP (2008) An evaluation of remote sensing techniques for enhanced detection of the toxic dinoflagellate, *Karenia brevis* . Remote Sens Environ 113:598- 609

Walsh JJ, Jolliff JK, Darrow BP, Lenes JM, Milroy SP, Remsen A, Dieterle DA, Carder KL, Chen FR, Vargo GA, Weisberg RH, Fanning KA, Muller-Karger FE, Shinn E, Steidinger KA, Heil CA, Tomas CR, Prospero JS, Lee TN, Kirkpatrick GJ, Whitledge TE, Stockwell DA, Villareal TA, Jochens AE, Bontempi PS (2006) Red tides in the Gulf of Mexico: Where, when, and why? J Geophys Res 111: 111: C11003, doi:10.1029/2004JC002813

Walsh JJ, Steidinger KA (2001) Saharan dust and Florida red tides: The cyanophyte connection. J Geophys Res 106:11597-11612

Walsh JJ, Weisberg RH, Lenes JM, Chen FR, Dieterle DA, Zheng L, Carder KL, Vargo GA, Havens JA, Peebles E, Hollander DJ, He R, Heil CA, Mahmoudi B, Landsberg JH (2009) Isotopic evidence for dead fish maintenance of Florida red tides, with implications for coastal fisheries over both source regions of the West Florida shelf and within downstream waters of the South Atlantic Bight. Prog Oceanogr 80:51-73

Zhang H (2002) Detecting Red Tides on the West Florida Shelf by Classification of SeaWiFS Satellite Imagery. Master's thesis, Department of Computer Science and Engineering, University of South Florida, December 2002